The Impact of Antenna Height on 3D Channel: A Ray Launching Based Analysis

Qi Hong [1],* [ID] **, Jiliang Zhang [2], Hui Zheng [1], Hao Li [1], Haonan Hu [1], Baoling Zhang [1], Zhihua Lai [3] and Jie Zhang [1,3]**

[1] Department of Electronic and Electrical Engineering, University of Sheffield, Sheffield S10 2TN, UK; hzheng6@sheffield.ac.uk (H.Z.); hli33@sheffield.ac.uk (H.L.); haonan.hu@sheffield.ac.uk (H.H.); bzhang13@sheffield.ac.uk (B.Z.); jie.zhang@sheffield.ac.uk (J.Z.)
[2] Information Science and Engineering Department, Lanzhou University, Lanzhou 730000, China; zhangjiliang@lzu.edu.cn
[3] Ranplan Wireless Network Design Ltd., Cambridgeshire CB23 3UY, UK; zhihua.lai@ranplanwireless.com
* Correspondence: qhong2@sheffield.ac.uk; Tel.: +44-744-790-0312

Abstract: Three-dimensional (3D) multi-input-multi-output (MIMO) is one of the enabling technologies for next-generation mobile communication. As the elevation angle in the 3D MIMO channel model might vary against the height of the base station (BS) antenna, it should be considered within channel modeling. In this paper, the impact of antenna height on the channel characteristics of the 3D MIMO channel is investigated by using the intelligent ray launching algorithm (IRLA). Three typical street scenarios, i.e., the straight street, the forked road, and the crossroad, are selected as benchmarks. The joint and marginal probability density functions (PDFs) of both the elevation angle of departure (EAoD) and the elevation angle of arrival (EAoA) are obtained through simulations. Moreover, the elevation angle spread (AS) and the elevation delay spread (DS) under various antenna heights are jointly discussed. Simulation results show that the characteristics of the PDFs of EAoD will vary under different street scenarios. It is observed that in order to obtain the maximum or minimum value of the AS and the DS, the BS antenna should be deployed at half of the building height.

Keywords: 3D; elevation angle; antenna height; elevation angle of departure; elevation angle of arrival; angle spread; delay spread

1. Introduction

One common feature of the research works on future wireless communication technologies is the pursuit of high spectral efficiency whilst multiple mobile stations (MSs) access the network. Multi-user (MU), multi-input-multi-output (MIMO) technology is expected to play a key role to achieve high spectral efficiency [1]. To thoroughly investigate MIMO, it is essential to have a good understanding of radio-propagation characteristics of transmission path between the base station (BS) and the MS [2]. Several models are proposed to describe the radio channel [3–5]. In [3,4], the authors analyzed the channel characteristics by assuming the scatters are located uniformly within a circle or an ellipse. In [5], the authors argued that stochastic geometry and random graph theory are indispensable tools for the analysis of wireless networks. For the conventional study on channel model, linear antenna arrays were employed in the horizontal direction [6–8]. This assumption is valid since the distance between the MS and the BS is much larger than the distance between the height of the BS antenna and the scatterers around the MS [9].

However, considering 3D distributed MSs, a better coverage and capacity can be achieved by using a 3D antenna array [10]. Under this condition, the elevation angle of departure (EAoD) and elevation angle of arrival (EAoA), which significantly affect the performance of MU-MIMO, should

be considered for channel modeling. The original EAoD and EAoA model was proposed in [11]. In 1990, a measurement in Tokyo based on 900 MHz observed that the distribution of elevation angle is extremely close to be Gaussian [12]. In 2002, the PDF of the EAoD for multipath at the BS was derived by assuming that the scattering objects were located uniformly within a circle around the MS [13]. Then, more research works started to appear over 10 years later. In [14], the spatial channel model (SCM) was extended to 3D by considering the elevation angle at the MS. In [15], a 3D scattering model was generalized for the macrocell environment with an MS located at the center of a 3D scattering semispheroid and a BS employing a directional antenna, which is located outside of the semispheroid. Recently, the scattering behavior was studied in [16]. Some other works focusing on the elevation angle in different propagation environments can be found in [17,18]. In [17], a new expression, which directly relates the PDF of the elevation angle, was proposed to the power spectral density of the received signal. In [18], the authors applied a novel technique for measuring the angular distribution in different environments. Although previous works have analyzed the distribution of the EAoD and the EAoA, the impact of antenna height on the EAoD and the EAoA has not been considered.

Ultra-dense small cells, with various antenna heights, are widely investigated in 5G networks. Due to small coverage areas, the impact of antenna height on parameters of wireless propagation, especially the EAoD and the EAoA, becomes significant. Previous work indicated that the heights of the antennas at both the BS and the MS impact \ the distribution of EAoD and EAoA significantly [19]. However, they did not consider how the antenna height would affect the distribution of elevation angle.

The main contributions of this paper are as follows. Firstly, the EAoD and the EAoA are characterized under typical scenarios against heights of antennas. Secondly, the PDFs of EAoD and EAoA are derived in closed-forms under each scenario. From the derived PDFs, we observe that the PDFs of EAoD and EAoA are almost linearly correlated with the antenna height under the straight street scenario. Meanwhile, the characteristics of PDFs change dramatically when the BS antenna height is half of the building's height under the forked road and crossroad scenarios. Finally, the effects of antenna height on the AS and the DS under the three typical scenarios are also discussed. We conclude that the AS and the DS reach their maximum or minimum value when the antenna height is half of the building's height, except the AS under the crossroad scenario.

This paper is organized as follows. In Section 2, we briefly introduce the IRLA and the experiment scenarios. In Section 3, we derive the PDFs of EAoD and EAoA under experiment scenarios through simulations. Meanwhile, the AS and DS are also analyzed. Finally, some conclusions are drawn in Section 4.

2. Methods and Numerical Results

2.1. Intelligent Ray Launching Algorithm (IRLA)

Radio wave propagation prediction modeling is critical in wireless network planning and optimization [20]. Types of propagation models have been presented in decades which can be classified as empirical models and deterministic models [21–23]. On the one hand, the channel characteristics in empirical models are determined by empirical factors, such as the carrier frequency and the distance between the BS and the MS. These models are time-efficient but with lower accuracy. On the other hand, deterministic models mainly consider the environmental information, such as the position and the reflection factor of the buildings. Thus, they are time consuming, but with higher accuracy [24]. The IRLA in our research can be categorized as a deterministic approach. The IRLA is used to compute all the possible reflections and diffractions of the emitting rays from the BS. Once the rays undergo reflections or diffractions, the additional loss will be added to the corresponding signal strength [25].

In [26], the authors originally presented the IRLA model, which relays on the cubic data obtained from discretization of the environment. The building walls, ground, and trees can be regarded as a cube element. Each cube is associated with a set of information. Then the authors proposed and implemented the parallel IRLA based on parallel object-oriented programming in C++ [27].

The IRLA contains three main components: light-of-sight (LOS), vertical diffraction (VD) and horizontal diffraction and reflection (HDR). The LOS component is used to calculate the path which is visible to emitter. The VD component is responsible for finding the roof-top diffractions rays. The HDR component is the most complicated part which launches a complete set of combination of diffraction and reflection rays. In [28], the authors implemented the angular dispersion of ray launching to improve its accuracy. Moreover, the model was extended to indoor scenarios in [29] and the combination with other methods was given in [30,31]. The correction of the IRLA model is justified in [29] and [32–34]. A measurement test in [29] showed the indoor IRLA model is promising with accurate results and time saving. Meanwhile, the accuracy of the model under an indoor-to-outdoor scenario and outdoor-to-indoor scenario were validated in measurements [32,33]. Recently, analysis and comparison between the simulation results and measurements showed that the ray-launching methods are efficient and accurate for massive MIMO channel modelling [34].

2.2. Numerical Results

The simulation scenario is part of the center of Paris, as shown in Figure 1. The size of the area is 500 m × 300 m, and the average building height is approximately 21 m [35]. We configure the transmit power of the BS as 0 dBm and the carrier frequency as 2.4 GHz (these two values can be set as any reasonable values at low frequency). For sake of convenience, we regard there are 4 × 1 omnidirectional antennas arranged in horizontal plane in the BS. The maximum reflection and diffraction numbers are 3 and 7, respectively. The parameters are listed in Table 1.

Table 1. Parameter settings of the experimental scenarios.

Size of Area	Average Buildings Height	BS Power	Carrier Frequency	BS Antenna Type	Max Reflection Number	Max Diffraction Number
500 m × 300 m	21 m	0 dBm	2.4 GHz	Omnidirectional 4 × 1	3	7

Figure 1 illustrates that there are three typical street scenarios: a straight street (red rectangular area), a forked road (black rectangular area), and a crossroad (dark red rectangular area) [36]. These three typical scenarios are displayed in Figure 2 and the parameters for each scenario are listed in Table 2. During simulations, *h* is the height of the BS, and *n* is the index of MSs from 1 to 100,000, which means 100,000 receivers are uniform distributed around the BS in total. We deployed the BS at $(0, 0, h)$ and the receivers at (x_n, y_n, z_n) in the global coordinate system. We regard the angles above the antenna height as having a negative degree (<0°), and the angles below the antenna height as a positive degree (>0°). Without loss of accuracy, we have not considered the direct component.
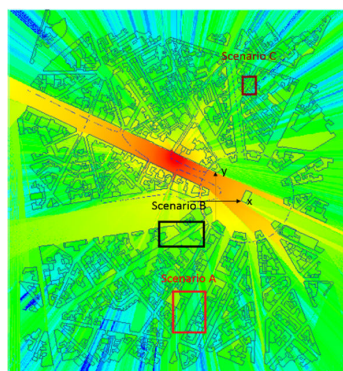

Figure 1. Part of the center of Paris (the red rectangular area, the black rectangular area, and the dark red rectangular area represent one of the straight streets, forked roads, and crossroads, respectively) [35].
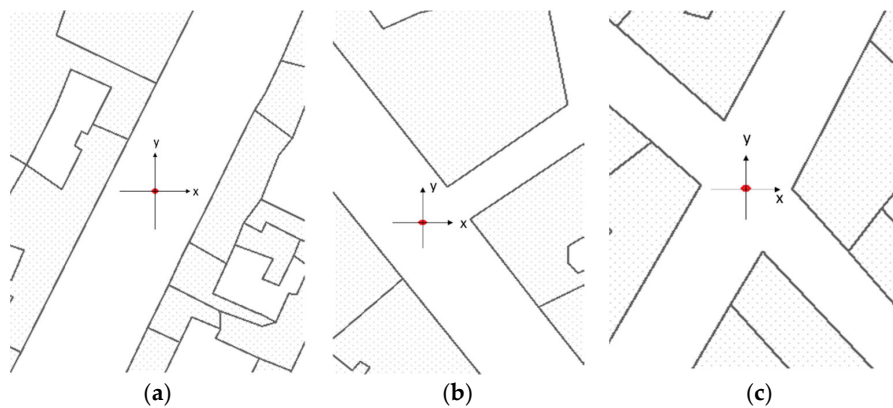
Figure 2. Three typical scenarios: (**a**) description of the straight street; (**b**) description of the forked road; and (**c**) description of the crossroad.

Table 2. Parameters of the three scenarios.

	Average Buildings Height	Length of Wider Street	Width of Wider Street	Length of Lower Street	Width of Lower Street
Straight street	20 m	80 m	20 m	0 m	0 m
Forked road	25 m	80 m	20 m	40 m	12 m
Crossroad	22 m	40 m	20 m	40 m	12 m

3. Results

3.1. Scenario A: Straight Street in the Center of Paris

Under the straight street in Figure 2a, the PDFs of EAoD and EAoA are investigated firstly. Due to reflection and diffraction during the signal transmission, each receiver can obtain multiple rays with different path losses, EAoDs and EAoAs. The PDFs of EAoD and EAoA can then be calculated after adding the weighting value (path loss).

Two simulation results, antenna heights at 8 m and 12 m, are indicated above. Figure 3 indicates that the PDF values of both the EAoD and EAoA around 0 radians are obviously greater than the values away from 0 degrees, and the sub-curves at the negative and positive are asymmetrical, which have been verified in [18]. The author observed that a double-sided exponential function is more suitable for the PDF of elevation angles which can be represented as:

$$f_{EAOD}(x) = \begin{cases} \lambda_{1EAOD}e^{-\lambda_{1EAOD}x}, & x < 0 \\ \lambda_{2EAOD}e^{-\lambda_{2EAOD}x}, & x > 0 \end{cases} \tag{1}$$

$$f_{EAOA}(x) = \begin{cases} \lambda_{1EAOA}e^{-\lambda_{1EAOA}x}, & x < 0 \\ \lambda_{2EAOA}e^{-\lambda_{2EAOA}x}, & x > 0 \end{cases} \tag{2}$$

Here, the unit of x is degrees. λ_{1EAoD}, λ_{2EAoD}, λ_{1EAoA}, and λ_{2EAoA} are the rate parameters of these double-sided exponential functions. By logarithm fitting the PDFs of EAoD and EAoA (for example: $\lambda'_{1EAoD} = -10 \times \log_{10}e \times \lambda_{1EAoD}$), we can finally obtain the values of λ'_{1EAoD}, λ'_{2EAoD}, λ'_{1EAoA}, and λ'_{2EAoA}. In Figure 3: $\lambda'_{1EAoD} = 26.83$, $\lambda'_{2EAoD} = -36.48$, $\lambda'_{1EAoA} = 16.43$, $\lambda'_{2EAoA} = -15.69$. Obviously, the λ' will be different with various antenna heights.

In Figure 4, the λ' with various antenna heights (4–18 m) are listed. This illustrates that the logarithm exponent value are almost linearly correlated with the antenna height. Then, we can derive that: $\lambda'_{1EAoD} = 1.64 \times m + 14.35$, $\lambda'_{2EAoD} = 1.60 \times m - 48.83$, $\lambda'_{1EAoA} = -0.63 \times m + 22.84$, $\lambda'_{2EAoA} = -0.76 \times m - 9.55$, where m is the antenna height which unit is meter. As we can see

from Figure 4, the logarithm exponent values λ'_{1EAoD} and λ'_{2EAoD} (as shown in Equation (1)) linearly increase with the antenna height growing, and the exponent values λ'_{1EAoA} and λ'_{2EAoA} (as shown in Equation (2)) linearly decrease with the antenna height growing.
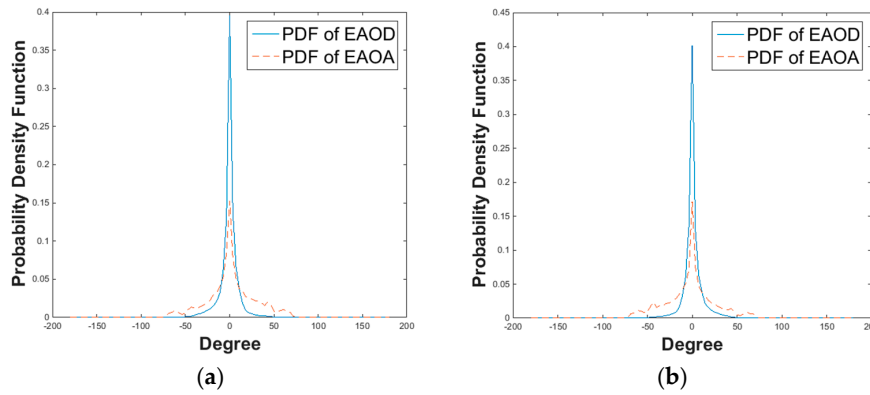

Figure 3. PDFs of EAoD and EAoA under the straight street scenario. (**a**) The description of the antenna height at 8 m; and (**b**) the description of the antenna height at 12 m.
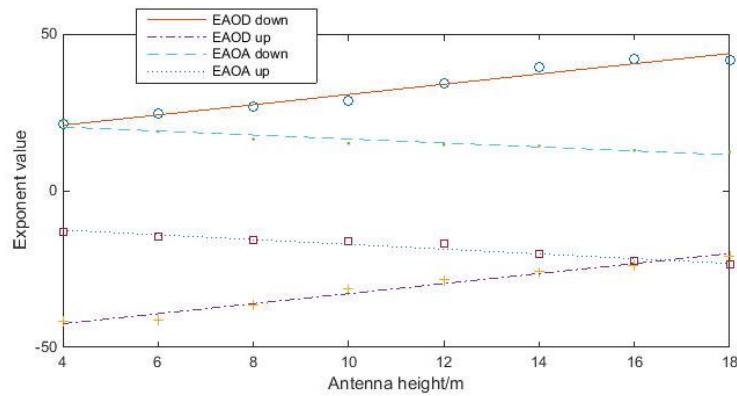

Figure 4. The statistic results of logarithm exponent values under straight street scenario with various antenna heights (4 m, 6 m, 8 m, 10 m, 12 m, 14 m,16 m, and 18 m), the EAoD down, EAoD up, EAoA down, and EAoA up represent λ'_{1EAoD}, λ'_{2EAoD}, λ'_{1EAoA}, and λ'_{2EAoA}, respectively.

Finally, the PDFs of EAoD and EAoA related to antenna height can be represented as:

$$f_{EAOD}(x) = \begin{cases} -(0.38m + 3.30)\exp(0.38m + 3.30), & x < 0 \\ -(0.37m - 11.24)\exp(0.37m - 11.24), & x > 0 \end{cases} \tag{3}$$

$$f_{EAOA}(x) = \begin{cases} -(-0.15m + 5.26)\exp(-0.15m + 5.26), & x < 0 \\ -(-0.18m - 2.20)\exp(-0.18m - 2.20), & x > 0 \end{cases} \tag{4}$$

Using the PDFs, the AS and the DS, which represent the elevation angle dispersion and the time dispersion of multipath components respectively, can be evaluated [13].

$$\sigma_{AS} = \sqrt{\frac{\sum_{i=1}^{L-1} P_i \theta_i^2}{\sum_{i=1}^{L-1} P_i} - \left(\frac{\sum_{i=1}^{L-1} P_i \theta_i}{\sum_{i=1}^{L-1} P_i}\right)^2} \tag{5}$$

$$\sigma_{DS} = \sqrt{\frac{\sum_{i=1}^{L-1} P_i \tau_i^2}{\sum_{i=1}^{L-1} P_i} - \left(\frac{\sum_{i=1}^{L-1} P_i \tau_i}{\sum_{i=1}^{L-1} P_i}\right)^2} \tag{6}$$

where P_i is the ray power, θ_i and τ_i are the angle and delay of ith ray. The statistic results of the AS and the DS are represented in Figures 5 and 6, respectively.
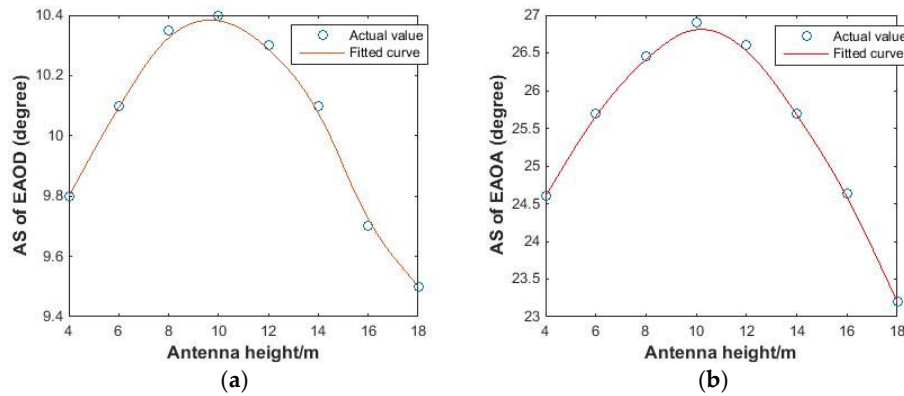

Figure 5. The AS under the straight street scenario with various antenna heights (4 m, 6 m, 8 m, 10 m, 12 m, 14 m, 16 m, and 18 m). (**a**) The description of the AS of EAoD; and (**b**) the description of the AS of EAoA.
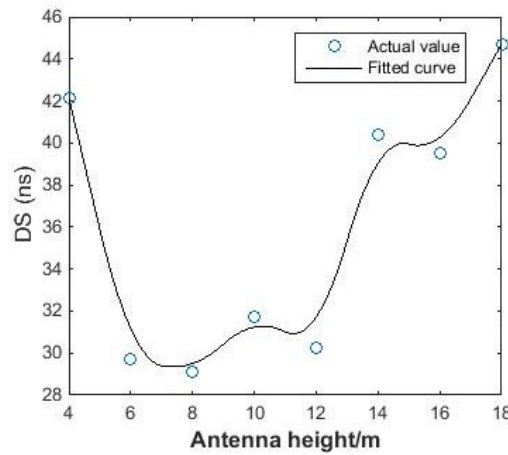

Figure 6. The DS with various antenna heights (4 m, 6 m, 8 m, 10 m, 12 m 14 m, 16 m, and 18 m).

Figure 5 indicates that the value of the AS of EAoD is smaller than that of EAoA, and the variation range of the AS of EAoD is also smaller. The AS reaches its maximum value when the antenna height (10 m) is half of the building's height. Figure 6 exhibits that the value of the DS is nearly unchangable when the antenna height is around half of the buildings height and increases conspicuously when the antenna is near the bottom or the top of the buildings.

By using the linear least square regression, we can obtain the correlation of the AS and DS with antenna height:

$$\sigma_{AS,EAOD} = \begin{cases} 0.1m + 9.4, & m \leq 10 \\ -0.11m + 11.5, & 10 < m \leq 20 \end{cases} \tag{7}$$

$$\sigma_{AS,EAOA} = \begin{cases} 0.383m + 23.07, & m \leq 10 \\ -0.4625m + 31.525, & 10 < m \leq 20 \end{cases} \tag{8}$$

$$\sigma_{DS} = \begin{cases} -2.905m + 53.74, & m < 8 \\ 30.5, & 8 \leq m \leq 12 \\ 2.3667m + 2.1, & 12 < m \leq 20 \end{cases} \tag{9}$$

where m is the antenna height. $\sigma_{AS,EAOD}$, $\sigma_{AS,EAOA}$, and σ_{DS} are the AS of EAoD, EAoA, and the DS, respectively.

3.2. Scenario B: Forked Road in the Center of Paris

Then, by using the same research steps in Section 3.1, we investigate the PDFs of EAoD and EAoA under the forked road scenario, as shown in Figure 2b. The simulation results when the antenna is located at 8 m and 12 m are indicated in Figure 7.
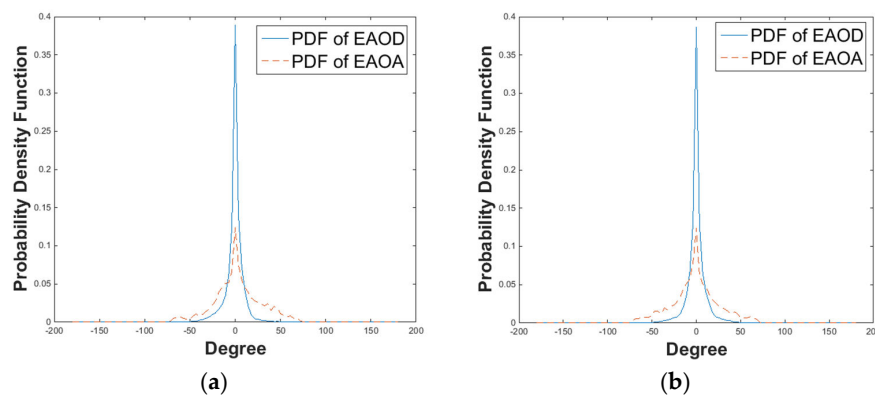

Figure 7. PDFs of EAoD and EAoA under the forked road scenario. (**a**) The description of the antenna height at 8 m; and (**b**) the description of the antenna height at 12 m.

After fitting the curves under different antenna heights (4 m, 6 m, 8 m, 10 m, 12 m, 14 m, 16 m and 18 m), the PDFs of EAoD and EAoA can be obtained as indicated in Table 3.

Table 3. The statistic results of logarithm exponent values under fork road scenario with various antenna heights (4 m, 6 m, 8 m, 10 m, 12 m, 14 m, 16 m, and 18 m). Here, EAoD down, EAoD up, EAoA down, and EAoA up represent λ'_{1EAoD}, λ'_{2EAoD}, λ'_{1EAoA}, and λ'_{2EAoA}, respectively.

	4 m	6 m	8 m	10 m	12 m	14 m	16 m	18 m
EAoD down	40.19	32.86	32.31	33.16	33.16	33.25	34.58	36.2
EAoD up	-32.49	-35.89	-34.23	-33.67	-32.63	-32.99	-32.93	-32.94
EAoA down	17.4	20.92	19.11	18	17.69	17.94	17.95	18.03
EAoA up	-18.06	-16.2	-15.77	-16	-17.06	-16.64	-16.45	-18.68

From Table 3, two conclusions can be reached:

- For the PDF of EAoD: the logarithm exponent value λ'_{1EAoD} is nearly unchangeable when the antenna height is lower than half of the building's height, but has a dramatic increase when the antenna height grows. However, the logarithm exponent value λ'_{2EAoD} enhances when the antenna height is lower than half of the building's height and then remains stable.
- For the PDF of EAoA: the logarithm exponent value λ'_{1EAoA} decreases rapidly when the antenna height is lower than half of the building's height and then varies slightly. However, the logarithm exponent value λ'_{2EAoA} is almost stable when the antenna height is lower than half of the building's height, but has a significant drop when the antenna height increases.

Finally, the PDFs of EAoD and EAoA related to antenna height can be calculated:

$$f_{EAOD}(x) = \begin{cases} -(7.64)\exp(7.64), & x < 0,\ m \le 12.5 \\ -(0.14m + 5.89)\exp(0.14m + 5.89), & x < 0,\ 12.5 < m < 25 \\ -(0.07m - 8.43)\exp(0.07m - 8.43), & x > 0,\ m \le 12.5 \\ -(-7.58)\exp(-7.58), & x > 0,\ 12.5 < m < 25 \end{cases} \tag{10}$$

$$f_{EAOA}(x) = \begin{cases} -(-0.06m + 4.87)\exp(-0.06m + 4.87), & x < 0, \ m \leq 12.5 \\ -(4.13)\exp(4.13), & x < 0, \ 12.5 < m < 25 \\ -(-3.80)\exp(-3.80), & x > 0, \ m \leq 12.5 \\ -(-0.06m - 3.01)\exp(-0.06m - 3.01), & x > 0, \ 12.5 < m < 25 \end{cases} \tag{11}$$

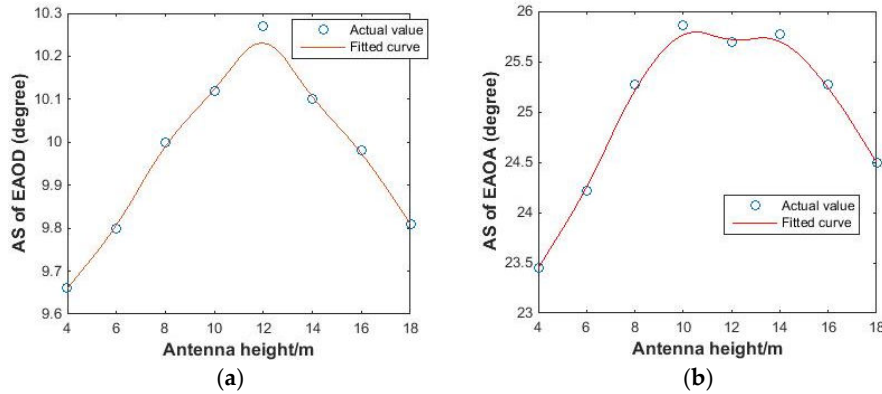With the results obtained above, the AS and the DS of EAoD and EAoA can be gained as displayed in Figures 8 and 9.

(**a**) (**b**)

Figure 8. The AS under the forked road scenario with various antenna heights (4 m, 6 m, 8 m, 10 m, 12 m, 14 m, 16 m, and 18 m). (**a**) The description of the AS of EAoD; and (**b**) the description of the AS of EAoA.
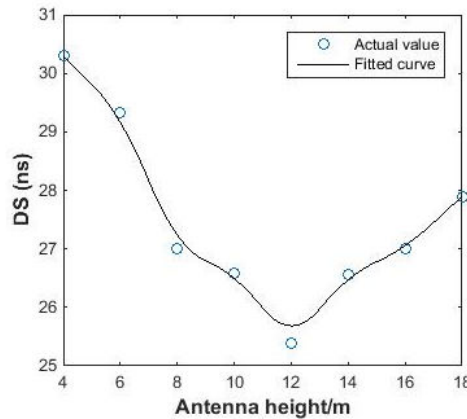

Figure 9. The DS under the forked road scenario with various antenna heights (4 m, 6 m, 8 m, 10 m, 12 m, 14 m, 16 m, and 18 m).

It is obvious from Figure 8 that the ASs of EAoD and EAoA arrive at the peak value when the antenna height (12 m) is half of the building's height. In Figure 9, we can conclude that the minimum value of the DS can be achieved when the antenna height is half of the building's height and the value arises when the antenna is near the ground or the top of the buildings.

Finally, the AS and the DS related to antenna height can be represented as:

$$\sigma_{AS,EAOD} = \begin{cases} 0.0824m + 9.2706, & m \leq 12.5 \\ -0.1273m + 11.8909, & 12.5 < m \leq 25 \end{cases} \tag{12}$$

$$\sigma_{AS,EAOA} = \begin{cases} 0.2412m + 22.6853, & m \leq 12.5 \\ -0.2m + 28.2, & 12.5 < m \leq 25 \end{cases} \tag{13}$$

$$\sigma_{DS} = \begin{cases} -0.5647m + 32.5588, & m \le 12.5 \\ 0.4364m + 20.0455, & 12.5 < m \le 25 \end{cases} \tag{14}$$

3.3. Scenario C: Crossroad in the Center of Paris

Finally, we research the PDFs of EAoD and EAoA under cross road scenario as shown in Figure 2c. The simulation results are obtained when the antenna located at 8 m and 12 m as shown in Figure 10.
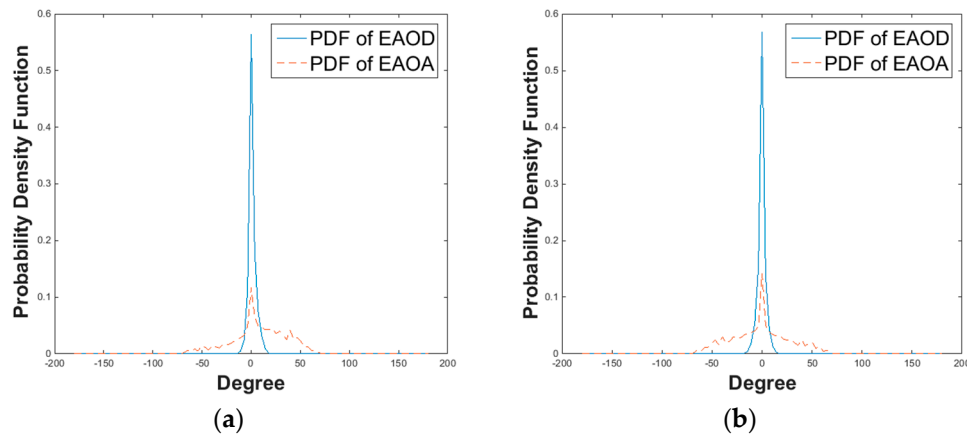

Figure 10. PDFs of EAoD and EAoA under the crossroad scenario. (**a**) The description of the antenna height at 8 m; and (**b**) the description of the antenna height at 12 m.

The logarithm exponent values of EAoD and EAoA can be obtained by fitting the curves through different antenna heights (4 m, 6 m, 8 m, 10 m, 12 m, 14 m, 16 m, and 18 m) which are exhibited in Table 4.

Table 4. The statistic results of logarithm exponent values under fork road scenario with various antenna heights (4 m, 6 m, 8 m, 10 m, 12 m, 14 m, 16 m, and 18 m). Here, EAoD down, EAoD up, EAoA down, and EAoA up represent λ'_{1EAoD}, λ'_{2EAoD}, λ'_{1EAoA}, and λ'_{2EAoA}, respectively.

	4 m	6 m	8 m	10 m	12 m	14 m	16 m	18 m
EAoD down	199	149.8	118.3	110.5	88.88	79.08	85.5	79.05
EAoD up	−79.57	−87.87	−76.54	−85.21	−103	−113.1	−131.2	−172.7
EAoA down	19.52	17.72	14.08	12.08	12.87	10.91	9.77	11.1
EAoA up	−9.556	−12.86	−10.7	−11.25	−13.12	−13.46	−15.32	−19.56

From Table 4, we can conclude that:

- For the PDF of EAoD: the logarithm exponent value λ'_{1EAoD} reduces rapidly when the antenna height is lower than half of the building's height, and gains the minimum value at 14 m, and then the value remains the same. In contrast, the logarithm exponent value λ'_{2EAoD} is nearly unchangeable when the antenna height is lower than half of the building's height, but has a dramatic decrease when the antenna height grows.
- For the PDF of EAoA: the exponent value decreases λ'_{1EAoA} as the antenna height rises. In contrast, the exponent value λ'_{2EAoA} is nearly unchanged when the antenna height is lower than half of the building's height, but has a significantly drop when the antenna height increases.

Then, the PDFs of EAoD and EAoA can be represented as:

$$f_{EAOD}(x) = \begin{cases} -(-2.95m + 52.22)\exp(-2.95m + 52.22), & x < 0, \ m \leq 11 \\ -(19.80)\exp(19.80), & x < 0, \ 11 < m < 22 \\ -(-20.72)\exp(-20.72), & x > 0, \ m \leq 11 \\ -(-1.90m + 0.15)\exp(-1.90m + 0.15), & x > 0, \ 11 < m < 22 \end{cases} \tag{15}$$

$$f_{EAOA}(x) = \begin{cases} -(-0.17m + 5.15)\exp(5.15), & x < 0, \ 0 < m < 22 \\ -(-2.76)\exp(-2.76), & x > 0, \ m < 11 \\ -(-0.15m - 1.08)\exp(-0.15m - 1.08), & x > 0, \ 11 < m < 22 \end{cases} . \tag{16}$$

The AS and the DS of EAoD and EAoA can be gained by the above results.

Figure 11a shows that the AS of EAoD remains almost stable with different antenna heights. Figure 11b illustrates the AS of EAoA gains its maximum value when the antenna height is half of the building's height (11 m) and drops gradually to the ground or the top of the buildings. The DS shows a similar phenomenon as that described in Sections 3.1 and 3.2 and as shown in Figure 12.
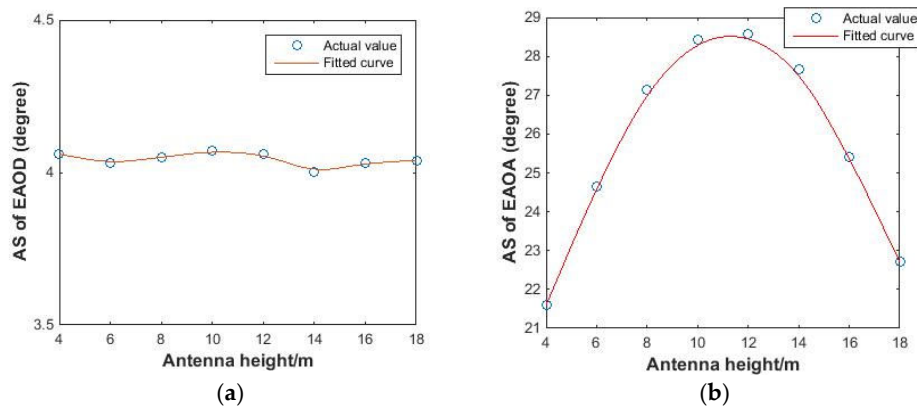

(a)   (b)

Figure 11. The AS under the crossroad scenario with various antenna heights (4 m, 6 m, 8 m, 10 m, 12 m, 14 m, 16 m, and 18 m). (**a**) Description of the AS of EAoD; and (**b**) a description of the AS of EAoA.
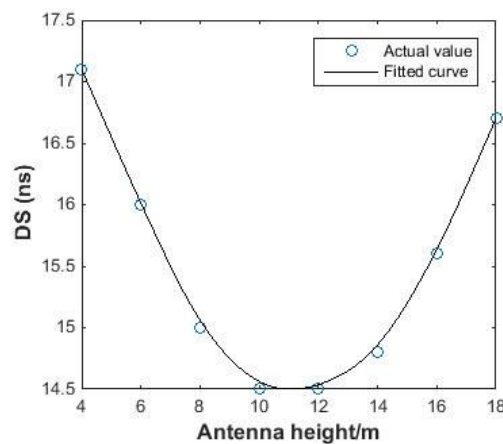

Figure 12. The DS under the crossroad scenario with various antenna heights (4 m, 6 m, 8 m, 10 m, 12 m, 14 m, 16 m, and 18 m).

Finally, the AS and the DS related to antenna height can be represented as:

$$\sigma_{AS,EAOD} = 4.05 \tag{17}$$

$$\sigma_{AS,EAOA} = \begin{cases} 0.9857m + 17.7571, & m \le 11 \\ -0.9m + 23, & 11 < m \le 22 \end{cases} \tag{18}$$

$$\sigma_{DS} = \begin{cases} -0.3571m + 18.4286, & m \le 12.5 \\ 0.3m + 11.2, & 11 < m \le 22 \end{cases} \tag{19}$$

3.4. Discussion

Based on the simulation results in Sections 3.1–3.3, some insights and observations regarding the 3D wireless channels are given as follows. On the one hand, to obtain the maximum and minimum values of the AS and the DS, BS antennas need to be located at half of the building's height under three typical street scenarios. On the other hand, the PDFs of EAoD and EAoA are approximated as double-sided exponential functions. Meanwhile, the parameters of the double-sided exponential function are linearly correlated with the antenna height under the straight street scenario, but change dramatically when the BS antenna height is half of the buildings height under forked road and crossroad scenarios.

Furthermore, from Figures 3, 7, and 10 we can find that most numbers of EAoD and EAoA concentrate at 0 radians, even though we ignore the direct component. Generally, the path distance of a single reflection angle is smaller than the multi-path which makes the weighting value higher. Thus, we can conclude that the single reflection path plays a leading role for researching the distributions of EAoD and EAoA.

4. Conclusions

In this paper, the impact of antenna height on EAoD and EAoA is investigated under typical outdoor scenarios: straight street, fork road, and crossroad. At the beginning, we briefly introduced the IRLA and the simulation scenario (the center of Paris). Then, the closed-form expressions of the PDF of EAoD and EAoA were derived under various street scenarios, the related AS and DS are also presented. Finally, the discussion of the results was given. According to the results, we conclude that the PDFs of EAoD and EAoA are modelled as exponential functions whose parameters are observed as a linear function of the antenna height under the straight street scenario. Meanwhile, the characteristics of EAoD and EAoA change dramatically when the BS antenna height is half of the building's height in the forked road and crossroad scenarios. Moreover, the results of the AS and the DS show that in order to obtain the maximum or minimum value of the AS and the DS, the BS antenna should be deployed at half of the building's height. We also conclude that the single reflection path dominates the distribution of EAoD and EAoA. In our future works, the PDFs of EAoD and EAoA with different antenna patterns and tilt will be considered under typical outdoor scenarios.

Author Contributions: Qi Hong, Jiliang Zhang, and Hui Zheng conceived and designed the experiments; Jiliang Zhang, Hui Zheng, and Hao Li performed the experiments; Qi Hong and Jiliang Zhang analyzed the data; Zhihua Lai and Haonan Hu contributed reagents/materials/analysis tools; and Qi Hong, Baoling Zhang, and Jie Zhang wrote the paper.

Conflicts of Interest: The authors declare no conflict of interest.

References

1. David, L.P.; Guvenc, I.; de la Roche, G.; Kountouris, M.; Quek, T.Q.S.; Zhang, J. Enhanced intercell interference coordination challenges in heterogeneous networks. *IEEE Wirel. Commun.* **2011**, *18*, 22–30.
2. Almesaeed, R.N.; Ameen, A.S.; Mellios, E.; Doufexi, A.; Nix, A. 3D channel models: Principles, Characteristics, and System Implications. *IEEE Commun. Mag.* **2017**, *55*, 152–159. [CrossRef]

3. Ertel, R.B.; Reed, J.H. Angle and time of arrival statistics for circular and elliptical scattering models. *IEEE J. Sel. Areas Commun.* **1999**, *11*, 1829–1840. [CrossRef]

4. Khan, N.M.; Simsim, M.T.; Rapajic, P.B. A generalized model for the spatial characteristics of the cellular mobile channel. *IEEE Trans. Veh. Technol.* **2008**, *1*, 22–37. [CrossRef]

5. Haenggi, M.; Andrews, J.G.; Baccelli, F.; Dousse, O.; Franceschetti, M. Stochastic geometry and random graphs for the analysis and design of wireless networks. *IEEE J. Sel. Areas Commun.* **2009**, *7*, 1029–1046. [CrossRef]

6. Molisch, A.F. Modeling of directional wireless propagation channels. *URSI Radio Sci. Bull.* **2002**, *302*, 16–26.

7. Jakes, W.C.; Cox, D.C. *Microwave Mobile Communications*; Wiley-IEEE Press: New York, NY, USA, 1994.

8. Mahmoud, S.S.; Hussain, Z.M.; Peter, O.S. A space-time model for mobile radio channel with hyperbolically distributed scatterers. *IEEE Antennas Wirel. Propag. Lett.* **2002**, *1*, 211–214. [CrossRef]

9. Alsehaili, M.; Noghanian, S.; Buchan, D.A.; Sebak, A.R. Angle-of-Arrival statistics of a three-dimensional geometrical scattering channel model for indoor and outdoor propagation environments. *IEEE Antennas Wirel. Propag. Lett.* **2010**, *9*, 946–949. [CrossRef]

10. Kammoun, A.; Khanfir, H.; Altman, Z.; Debbah, M.; Kamoun, M. Preliminary results on 3DD channel modelling: From theory to standardization. *IEEE J. Sel. Areas Commun.* **2014**, *32*, 1219–1229. [CrossRef]

11. Aulin, T. A modified model for the fading Signal at a mobile radio channel. *IEEE Trans. Veh. Technol.* **1979**, *28*, 182–203. [CrossRef]

12. Taga, T. Analysis for mean effective gain of mobile antennas in land mobile radio environments. *IEEE Trans. Veh. Technol.* **1990**, *39*, 117–131. [CrossRef]

13. Petrus, P.; Reed, J.H.; Rappaport, T.S. Geometrical-based statistical macrocell channel model for mobile environments. *IEEE Trans. Commun.* **2002**, *3*, 495–502. [CrossRef]

14. Shafi, M. The impact of elevation angle on MIMO capacity. In Proceedings of the IEEE International Conference on Communications, Istanbul, Turkey, 11–15 June 2006; pp. 4155–4160.

15. Nawaz, S.J. A generalized 3-D scattering model for a macrocell environment with a directional antenna at the BS. *IEEE Trans. Veh. Technol.* **2010**, *7*, 3193–3204. [CrossRef]

16. Tzarouchis, D.C.; Ylä-Oijala, P.; Sihvola, A. Resonant scattering characteristics of homogeneous dielectric sphere. *IEEE Trans. Antennas Propag.* **2017**, *6*, 3184–3191. [CrossRef]

17. Qu, S.; Yeap, T. A Three-dimensional scattering model for fading channels in land mobile environment. *IEEE Trans. Veh. Technol.* **1999**, *3*, 765–781.

18. Kalliola, K.; Sulonenet, K.; Laitinen, H.; Kivekas, O.; Krogerus, J.; Vainikainen, P. Angular power distribution and mean effective gain of mobile antenna in different propagation environments. *IEEE Trans. Veh. Technol.* **2002**, *5*, 823–838. [CrossRef]

19. Mondal, B.; Thomas, T.A.; Visotsky, E.; Vook, F.W.; Ghosh, A.; Nam, Y.-H.; Li, Y.; Zhang, J.; Zhang, M. 3D channel model in 3GPP. *IEEE Commun. Mag.* **2015**, *3*, 16–23. [CrossRef]

20. Ballot, M. Radio-wave propagation prediction model tuning of land cover effects. *IEEE Trans. Veh. Technol.* **2014**, *8*, 3490–3498. [CrossRef]

21. Kurner, T. *Radio Wave Propagation Part One "Theoretical Aspects"*; COST2100 Training School: Wroclaw, Poland, 2008.

22. Lostanlen, Y. *Radio Wave Propagation Part Two "Practical Aspects"*; COST2100 Training School: Wroclaw, Poland, 2008.

23. Klepal, M. Novel Approach to Indoor Electromagnetic Wave Propagation Modelling. Ph.D. Thesis, Czech Technical University, Prague, Czech, 2003.

24. Janaswamy, R. Angle and time of arrival statistics for the Gaussian scatter density model. *IEEE Trans. Wirel. Commun.* **2002**, *3*, 488–497. [CrossRef]

25. Hoppe, R.; Wolfle, G.; Landsterfer, F. Accelerated ray optical propagation modelling for the planning of wireless communication networks. In Proceedings of the 1999 IEEE Radio and Wireless Conference, Denver, CO, USA, 1–4 August 1999.

26. Lai, Z.; Bessis, N.; de la Roche, G.; Song, H.; Zhang, J.; Clapworthy, G. An intelligent ray launching for urban propagation prediction. In Proceedings of the 3rd European Conference on Antennas and Propagation, Berlin, Germany, 23–27 March 2009; pp. 2867–2871.

27. Lai, Z.; Bessis, N.; Kuonen, P.; de la Roche, G.; Zhang, J.; Clapworthy, G. A performance evaluation of a grid-enabled object-oriented parallel outdoor ray launching for wireless network coverage prediction. In Proceedings of the Fifth International Conference on Wireless and Mobile Communications, Cannes, France, 23–29 August 2009; pp. 38–43.

28. Lai, Z.; Bessis, N.; de la Roche, G.; Kuonen, P.; Zhang, J.; Clapworthy, G. A new approach to solve angular dispersion of discrete ray launching for urban scenarios. In Proceedings of the Loughborough Antennas & Propagation Conference, Loughborough, UK, 16–17 November 2009; pp. 133–136.

29. Lai, Z.; Bessis, N.; de la Roche, G.; Kuonen, P.; Zhang, J.; Clapworthy, G. The characterisation of human-body influence on indoor 3.5 GHz path loss measurement. In Proceedings of the 2010 IEEE Wireless Communications and Networking Conference Workshops (WCNCW), Sydney, Australia, 18 April 2010.

30. Umansky, D.; de la Roche, G.; Lai, Z.; Villemaud, G.; Gorce, J.-M.; Zhang, J. A new deterministic hybrid model for indoor-to-outdoor radio coverage prediction. In Proceedings of the 5th European Conference on Antennas and Propagation (EUCAP), Rome, Italy, 11–15 April 2011; pp. 3771–3774.

31. de la Roche, G.; Flipo, P.; Lai, Z.; Villemaud, G.; Zhang, J.; Gorce, J.-M. Combination of geometric and finite difference models for radio wave propagation in outdoor to indoor scenarios. In Proceedings of the Fourth European Conference on Antennas and Propagation (EuCAP), Barcelona, Spain, 12–16 April 2010.

32. de la Roche, G.; Gorce, J.-M.; Zhang, J. Optimized implementation of the 3D MR-FDPF method for indoor radio propagation prediction. In Proceedings of the 3rd European Conference on Antennas and Propagation, Berlin, Germany, 23–27 March 2009.

33. de la Roche, G.; Flipo, P.; Lai, Z.; Villemaud, G.; Zhang, J.; Gorce, J.-M. Implementation and validation of a new combined model for outdoor to indoor radio coverage predictions. *Wirel. Commun. Netw.* **2010**, *2010*, 215352. [CrossRef]

34. Weng, J.; Tu, X.; Lai, Z.; Salous, S.; Zhang, J. LaiIndoor Massive MIMO Channel Modelling Using Ray-Launching Simulation. *Int. J. Antenna Propag.* **2014**, *2014*, 279380. [CrossRef] [PubMed]

35. Ranplan. The Role and Benefits of RF and Performance Modelling Tools in the HetNet Era. White Paper. 2015. Available online: https://ranplanwireless.com/wp-content/uploads/The-Role-and-Benefits-of-RF-and-Performance-Modelling-tools-in-HetNet-Era.pdf (accessed on 7 November 2017).

36. Donikian, S. Vuems: A virtual urban environment modelling system. In Proceedings of the Computer Graphics IntHasselt and Diepenbeek, Belgium, Hasselt and Diepenbeek, Belgium, 23–27 June 1997; pp. 84–92.